ACS APPLIED MATERIALS & INTERFACES

Research Article

www.acsami.org

Nanopatterning Palladium Surface Layers through Electrochemical Deposition and Dissolution of Zinc in Ionic Liquid

Junhua Jiang,* Lei Zhang, and Xinying Wang

Illinois Sustainable Technology Center, University of Illinois at Urbana−Champaign, Champaign, Illinois 61820, United States

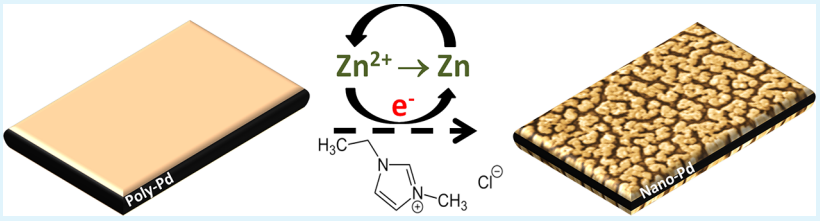

ABSTRACT: Cracklike nanopatterned palladium surface layers have been produced by a green chemistry method based on in situ electrochemical deposition-dissolution of zinc (Zn-ECDD) in an ionic liquid bath. During the cathodic process, reactive Zn was electrochemically deposited onto a polycrystalline Pd substrate. During the subsequent anodic process, Zn was removed from the substrate through electrochemical dissolution. Scanning electron microscope (SEM) measurements showed that repetitive Zn-ECDD mediated by potential cycles results in the nanopatterning of Pd surface layers, characterized by uniform crack appearance with well-distributed concave spacings separated by nanowidth cracks. Energy-dispersive X-ray microscopy (EDX) studies revealed that the nanopatterned surface layers chemically contain a small amount of Zn. A mechanism based on the development of stress induced by the Zn-ECDD on Pd surfaces was proposed to be responsible for the nanopatterning of Pd surface layers. Electrochemical oxidation of formic acid and reduction of nitrite were studied as model reactions to demonstrate potential applications of the nanopatterned Pd electrode to electrocatalysis and electrochemical determination of environmental contaminants. Highly improved electrochemical responses were obtained on the nanopatterned Pd for the two reactions, compared to the untreated Pd.

KEYWORDS: *nanopatterned palladium, electrochemical deposition-dissolution, ionic liquid, oxidation of formic acid, Nitrite reduction*

1. INTRODUCTION

Incorporation of nanostructures into metallic electrode surface layers is of particular interest for a wide range of potential applications, for example, electrochemical catalysis, because the nanostructures not only can increase the active area accessible to reactant molecules but also can improve electron mobility in the solid ligaments.[1−3] Other applications have been explored, such as electrochemical sensors[4,5] and energy storage-conversion systems.[6−8] However, controlling the nanoarchitecture of electrode surface layers faces great challenges since metals at the nanoscale favor low surface areas to minimize the surface energy. In the past two decades, several strategies have been developed to design and fabricate nanostructured electrodes with highly ordered networks and high surface area.[9,10] The control over the nanostructures enables systematically experimental and theoretical studies of the electrode structure−activity relationship.

Nanostructured palladium (Nano-Pd) in varied patterns has been synthesized and studied as a promising material for catalytic applications,[11,12] energy storage-conversion,[13−15] hydrogen storage[16] and detection,[17,18] and electrochemical sensors.[19,20] Nano-Pd thin-films prepared by a soft templating approach exhibit ordered nanostructures characteristic of regular nanopores separated by nanothick walls.[20−22] But the demand of expensive high-quality soft template and subsequent template removal limit the implementation of this method. A hard template method used to prepare Nano-Pd thin films faces similar limitations, because a highly ordered porous silica or alumina template is normally used and its removal requires the use of caustic chemicals which is time-consuming and not environmentally friendly.[17,18] Recently, dealloying of Pd-alloys has been studied to prepare Nano-Pd thin films based on the removal of a reactive alloying element.[23,24] However, the need of Pd-based alloy as a precursor imposes different challenges. Direct attachment of Pd nanoparticles onto an electrode substrate is achievable through physical dispersion or chemical introduction of the nanoparticles .[25−27] However, uniform dispersion of individual nanoparticles requires complicated surface modification/manipulation, elaborate equipment, or a considerable amount of time. It is therefore of interest to develop a more convenient method to incorporate the nanostructures onto Pd surfaces.

Though-thickness crack networks are known to form in drying media and thin films with residual tensile stress, and have been observed in several systems,[28−33] including drying mud, polymer paints, aging woods, dielectric thin films, and

Received: September 19, 2013
Accepted: November 12, 2013
Published: November 12, 2013

 © 2013 American Chemical Society

even in monolayers of microspheres. The ubiquitous and intriguing crack patterns have attracted broad interest in understanding the mechanisms of crack evolution and pattern formation. Several models have been proposed to simulate the cracking behaviors caused by drying and other physical and chemical shrinkage processes.[34−36] A simple two-dimensional spring-block model developed by Leung and Neda successfully captured the essential features of corn-starch drying.[34] Recently, Li et al. modified the spring-block model to simulate crack formation in amorphous Si thin film electrodes as a result of electrochemical lithiation and delithiation cylces.[37] Their simulation and experimental results showed that the generated crack patterns strongly depend on the thin film thickness. It was interestingly found that the nanopatterns characteristic of concave-shaped spacings separated by nanowidth cracks were obtained for very thin films. These indicate that it is possible to nanostructure electrode surfaces by creating cracks inside the electrode surface layers based on a mechanism of the crack formation. In this work, we have studied electrochemical deposition-dissolution of Zn (Zn-ECDD) onto a polycrystalline Pd microdisc in an ionic liquid bath as a tool for this purpose because in situ electrodeposited Zn can interact with the substrate of some noble metals, such as Au, to form an intermetallic phase and then to be selectively removed during the subsequent anode process.[38,39] Zn insertion and dissolution induced volume change and stress result in the formation of surface cracks. Our SEM measurements show that repetitive Zn-ECDD mediated by potential cycles caused the nanopatterning of Pd surface layers. Uniform cracklike nanostructures with narrowly distributed concave spacings separated by nanocracks were observed. To our knowledge, this is the first report of producing Nano-Pd film with cracklike nanoarchitecture. We have further studied Nano-Pd as an electrocatlayst for electrochemcial oxidation of formic acid and for determination of nitrite. Highly improved electrochemical responses for the two reactions were obtained on the Nano-Pd electrode, compared to its precursor, a polycrystalline Poly-Pd electrode. The biggest advantages of the one-pot ECDD approach over traditional approaches are that it is convenient, no net chemicals are consumed, no costly templates are needed, and it is environmentally benign.

2. EXPERIMENTAL SECTION

A polycrystalline Pd (Poly-Pd) microdisc electrode was prepared by sealing a Pd wire of 100 μm in diameter (Alfa Aesar) into glass pipet tubing following a traditional heat-sealing procedure. The microdisc electrode was polished and then ultrasonically cleaned in acetone and deionized water before use. The Zn-ECDD on the microdisc was performed by applying potential cycles to the Pd microdisc electrode in an ionic liquid bath comprising of 40 mol % $ZnCl_2$ and 60 mol % 1-ethyl-3-methylimidazolium chloride (EMIC) with a Zn rod and a Ag wire as the counter and reference electrodes, respectively. During the ECDD, only the microdisc top surface is exposed to the ionic liquid with its side surface sealed in glassy insulator. The potential was cycled between −2.0 and 0.60 V at 100 mV s^{-1}, and the working temperature was controlled at 140 °C unless otherwise stated. The scanning electron microscope (SEM) and energy-dispersive X-ray (EDX) microscope measurements were performed using field-emission environmental scanning electron microscope operating at 15 kV equipped with an energy-dispersive spectroscopy.

Electrochemical characterizations of the Nano-Pd microelectrode were carried out in Ar-degassed 0.5 mol dm^{-3} H_2SO_4 at 100 mV s^{-1} with Pt flag as the counter electrode and a Ag/AgCl electrode as the reference electrode. Before each experiment, the electrodes were cleaned in 0.5 mol dm^{-3} H_2SO_4 by potential cycling between −0.22 and 1.08 V until reproducible curves were obtained. The electrocatalytic activity of the Nano-Pd electrode toward formic acid (HCOOH) was studied in 0.5 mol dm^{-3} HCOOH + 0.5 mol dm^{-3} H_2SO_4 by means of voltammetry and chronoamperometry. For studying electrochemical responses of Nano-Pd to nitrite, steady-state voltammograms and chronoamperograms were measured in degassed 0.5 mol dm^{-3} H_2SO_4 solution containing KNO_2 of controlled concentration. For the purpose of comparison, electrochemical oxidation of formic acid and nitrite reduction were also studied on the Poly-Pd microdisc electrode under similar conditions before undergoing the Zn-ECDD treatment.

3. RESULTS AND DISCUSSION

Figure 1 shows cyclic voltammograms for the Poly-Pd microdisc electrode in the bath of $ZnCl_2$ and EMIC as a function of the number of potential cycles between −2.0 and 0.60 V. In the negative scan during the first potential cycle, the onset potential for obvious Zn nucleation and growth on the Pd substrate is approximately −0.72 V vs Ag reference electrode. Two reduction waves, I_c at about −0.82 V and II_c at about −1.32 V, are observed in a potential range over −0.70 to −1.50 V before the reduction currents are substantially increased. In the positive scan, three anodic peaks (I_a at around −0.60 V, II_a and III_a) are generated over the potential from −1.0 to 0.40 V by the dissolution of Zn. These assignments are supported by the base cyclic voltammograms of the electrode in the EMIC bath without containing $ZnCl_2$ shown in the inset to Figure 1, which show no obvious cathodic and anodic peaks in the potential range of −1.5 to 0.40 V and a considerable increase of the cathodic currents commences at approximately −1.50 V. The three anodic peaks respond to continuous potential cycling in different patterns. The currents and potentials of peak I_a are less dependent upon the potential cycle. Peak II_a exhibits a slight current increase and an obvious potential shift. The significant current increase of peak III_a is accompanied by an obvious potential shift. These peak currents are maximized at the 10th potential cycle and they are not obviously altered with further potential cycling.

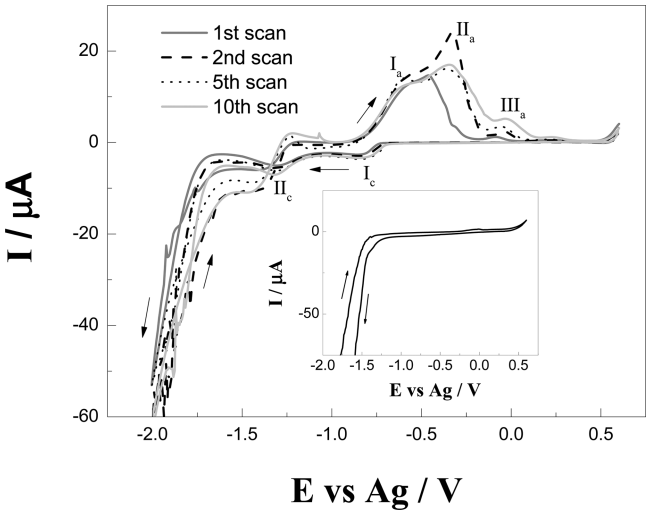

Figure 1. Cyclic voltammograms for a Poly-Pd electrode in an electrolyte bath of $ZnCl_2$ + EMIC as a function of the number of potential cycle between −2.0 and 0.6 V at 100 mV s^{-1}. Inset: Base voltammograms for the Poly-Pd electrode in an EMIC electrolyte under similar conditions.

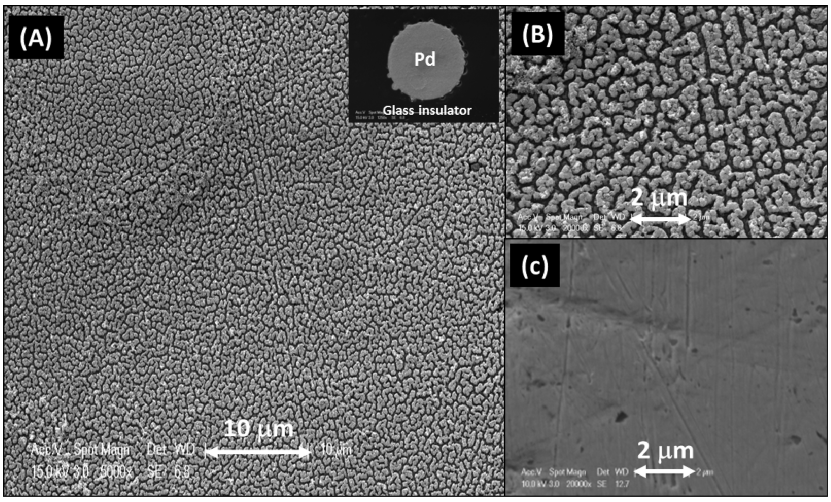

Figure 2. SEM images for Nano-Pd (A and B) and Poly-Pd (C). Inset to (A): Image of Nano-Pd microelectrode.

The SEM images of the untreated Poly-Pd microdisc and the resulting Nano-Pd electrode prepared by applying 15 potential cycles between −2.0 to 0.60 V at 100 mV s^{-1} are shown in Figure 2. The low-magnification image of the Nano-Pd electrode (Figure 2A and its inset) shows a uniform crack appearance. The high-magnification image (Figure 2B) highlights the nanotextures characteristic of concave spacings and interspacing cracks. They are obviously different from the morphology of the untreated Pd microdisc electrode exhibiting flat surfaces, straight scathes, and a few digs, as shown in Figure 2C. These are caused by mechanical polishing. The histograms for the concave spacings and the cracks are shown in Figure 3A and B, respectively. The width of the spacings ranges from around 150 to 400 nm with the frequency maximum seen at 250 nm. The width of the cracks falls within a narrow range from around 50 to 250 nm and reaches a maximum at 125 nm. The crack layer is very thin, around 230 nm in thickness. The average composition of the Nano-Pd layer measured using EDX spectroscope is approximately $Pd_{0.89}Zn_{0.11}$ by weight, indicating that a small amount of zinc is present in Pd. This suggests that electrodeposited Zn can interact with Pd surface layers. We have found that the residue Zn cannot be easily removed through successive potential scans between −0.22 and 1.08 V.

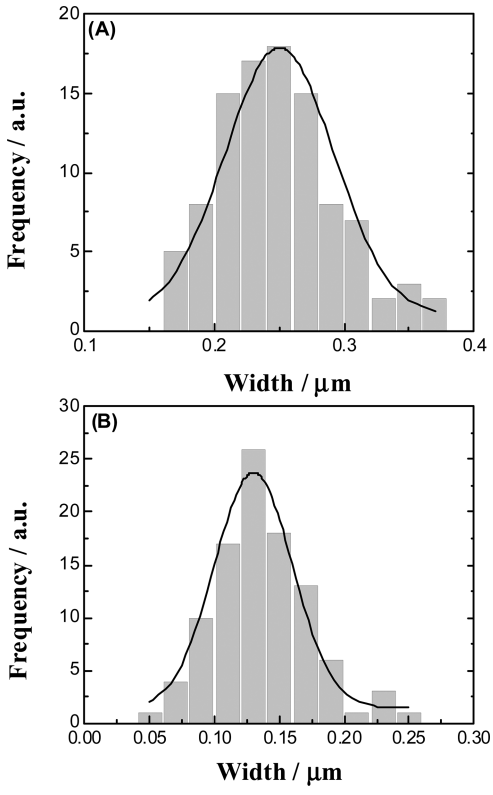

Figure 3. Histograms for width of concave spacings and width of cracks measured from Figure 2B.

Interestingly, the crack patterns observed in Figure 2 are very similar to those generated in a thin layer of cornstarch[36] and in amorphous Si thin film during electrochemical lithiation and delithiation cylces,[37] although Pd is a noble metal substantially different from amorphous Si and cornstarch. It is predictively and experimentally disclosed that the textures of the crack patterns strongly depend on the thickness of the substrate. Cracks generated in thick films are straight with a few sharp direction changes, and the area separated by crack is large. For thin films, cracks show more wiggles and the average crack area is small. In our case, the thickness of Pd thin film is around 230 nm, very close to the thickness of Si thin film (200 nm) used in the Li et al.'s simulation.[37] We have calculated the area of the cracks. It is around 7.5 μm^2, close to a theoretical value (7 μm^2) estimated from the scaling relationship between the average cracked area and the film thickness. Li et al. also found that the concave spacing exhibits a power-law scaling behavior between spacing area and perimeter. For the Nano-Pd film in our case, the area-perimeter scaling for the concave spacings separated by cracks is shown in Figure 4. The fractal dimension d_f which is defined as the power of area to perimeter is approximately 1.40, smaller than the value (1.57) for the 200 nm thick Si film. The lower value is indicative of more complicated patterns with concave edges. During Zn-ECDD, the insertion of Zn into Pd and its anodic dissolution from Pd may induce the volume change of surface layers and stress accumulation. It is reasonably postulated that the Pd disc outer layer is expanded upon the Zn insertion and shrunk after the Zn removal. Because the outer layer tries to shrink while the underlying layer is physically stable, a stress is developed and accumulates until it reaches a critical value: the yield stress. At the point

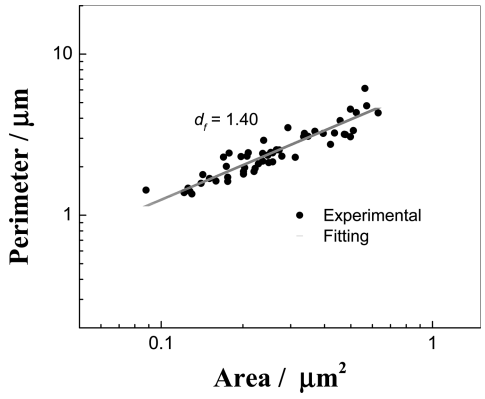

Figure 4. Area−perimeter scaling for concave spacings separated by cracks with data extracted from Figure 2B. The power-law fitting (in gray) gives a fraction dimension d_f = 1.40.

where the actual stress has exceeded the yield stress value, an initial fracture is introduced, forming a permanent discontinuity in the outer layer. As a result, the stress shifts to other regions of this layer which is likely to lie in the vicinity of the existing crack tips. This leads to crack propagation. Complicated patterns are formed if the propagation of cracks is stopped before reaching other crack branches.

Figure 5 shows electrochemical behavior of the Poly-Pd disc and Nano-Pd electrodes in 0.5 mol dm^{-3} H_2SO_4 in the

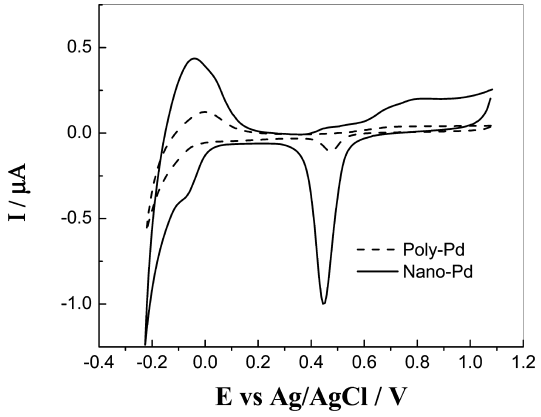

Figure 5. Cyclic voltammograms for a Nano-Pd 0.5 mol dm^{-3} H_2SO_4 at 100 mV s^{-1} (solid line), in comparison to those for a Poly-Pd electrode under the same conditions (dashed line).

potential range of −0.22 to 1.08 V vs Ag/AgCl. The characteristic electrochemical responses associated with hydrogen adsorption/desorption and oxide formation/reduction are clearly improved on Nano-Pd, compared to Poly-Pd. The roughness factor of the Nano-Pd electrode is estimated from the ratio of the charge associated with the oxide reduction corresponding to the sharp peak seen at around 0.45 V to a theoretical value of 420 μC cm^{-2} for the reduction of a PdO monolayer.[40] The calculated values are approximately 32 and 5.3 for Nano-Pd and Poly-Pd, respectively. This suggests that the electrochemical surface area of the electrode is significantly increased after Poly-Pd is treated via the Zn-ECDD. This agrees with the results of SEM measurements shown in Figure 2.

Pd has been the most active single metal electrocatalyst for electrochemical oxidation reaction of formic acid in acidic media which is the anode reaction of a direct formic acid fuel cell.[41−43] We studied the activities of Poly-Pd and Nano-Pd electrodes for this reaction. Figure 6 shows cyclic voltammo-

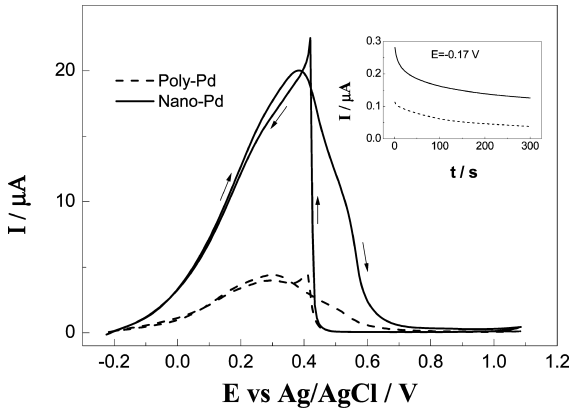

Figure 6. Cyclic voltammograms for a Nano-Pd (solid line) and a Poly-Pd (dash line) in 0.5 mol dm^{-3} HCOOH + 0.5 mol dm^{-3} H_2SO_4 at 100 mV s^{-1}. Inset: Current−time transients for the two electrodes taken after 300 s of polarization at −0.17 V vs Ag/AgCl.

grams for the two electrodes in 0.5 mol dm^{-3} HCOOH + 0.5 mol dm^{-3} H_2SO_4. The voltammetric characteristics of the two electrodes are similar over a wide potential range from −0.22 to 1.08 V, which is in agreement with literature results for HCOOH oxidation on Pd electrocatalysts in acidic media.[41,42] But the electrochemical responses are significantly higher on Nano-Pd than on Poly-Pd. The oxidation peak current measured in the positive scan is around 4 times higher for the former than the latter. The inset to this figure shows the variations of chronoamperometric current with polarization time after stepping the potential to −0.17 V (equivalent to 0.05 V vs RHE). The trends of the two current−time transients are similar and exhibit faster current decays at shorter times and slower current decays at longer times. But the chronoamperometric currents measured on the Nano-Pd electrode are much higher than those on the Poly-Pd electrode. Both voltammetric and chronoamperometric measurements show that Nano-Pd is more active than Poly-Pd toward the HCOOH oxidation, especially at potentials relevant to fuel cell operations.

Electrochemical reduction and determination of nitrite have attracted considerable attention since nitrite is an important contaminant in drinking water and their reaction kinetics are strongly dependent upon electrode microstructures.[44,45] Here, we have studied nitrite reduction in acidic media as the model reaction to demonstrate improved electrochemical responses of Nano-Pd over Poly-Pd. Figure 6 shows steady-state voltammograms for the Nano-Pd and Poly-Pd electrodes in 0.5 mol dm^{-3} H_2SO_4 containing 0.02 mol dm^{-3} KNO_2. Pseudolimiting currents are observed on the two electrodes. However, the value of limiting currents measured at 0.18 V on Nano-Pd is approximately 10 times higher than those on Poly-Pd. It is expected that the nanostructured microdisc electrode should exhibit a polarization behavior similar to that of a high-surface microelectrode which has been previously documented.[46] The nanostructured microelectrode can be approximated as a combination of a planar microdisc electrode of the same geometric diameter and a thin-layer electrochemical cell within the pores. Under diffusion control of bulk reactants, the electrochemical reaction is limited to occur at the outermost layer of the nanostructured microelectrode and the reaction within the pores is disabled since all reactant is consumed at the

outside layer and no reactant is available within the porous zones. Under this condition, the nanostructured microelectrode behaves as a normal microelectrode and there is no significant effect of the nanostructuration. In this work, the effective diameters of the Poly-Pd and Nano-Pd electrodes were almost the same. Apparently, the 10-times increase in the limiting currents on Nano-Pd over Poly-Pd cannot be attributed to the changes of macroscopic electrode geometry. Liu et al. have studied the nitrite reduction on high-surface catalysts in acidic media and concluded that the limiting-currents are controlled by a preceding chemical reaction rather than mass transport of bulk nitrite and can be substantially increased by increasing electrode surface area.[47] Our results clearly agree with their published results. Therefore, the increase of the electrode surface area caused by the nanostructuration of Poly-Pd into Nano-Pd is the origin of the unusual difference between their limiting currents in our case. During nitrite reduction, the preceding chemical reaction occurring before electron transfer can be written as follows:[47,48]

$$HNO_2 + H^+ \rightarrow NO^+ + H_2O \quad (1)$$

NO^+ is proposed to be the electroactive species directly accepting one electron from the electrode to be converted to NO as follows:

$$NO^+ + e^- \rightarrow NO \quad (2)$$

A theoretical Tafel slope of approximately 120 mV dec^{-1} will be expected if the electron transfer is the rate-determining step. The inset to Figure 7 shows the Tafel plots for nitrite reduction

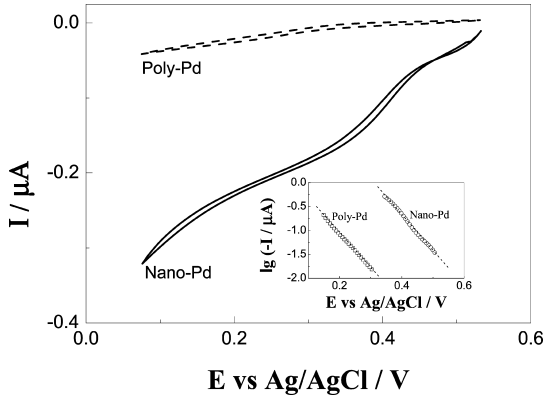

Figure 7. Steady-state voltammograms for a Nano-Pd (solid line) and a Poly-Pd (dashed line) in 0.02 mol dm^{-3} KNO_2 + 0.5 mol dm^{-3} H_2SO_4 at 5 mV s^{-1}. Inset: Tafel plots for nitrite reduction with data withdrawn from the negative scans.

on Poly-Pd and Nano-Pd. Experimental Tafel slopes measured from the linear Tafel plots are 140 and 136 mV dec^{-1} for Poly-Pd and Nano-Pd, respectively. Because these values are approximately in agreement with the theoretical value of 120 mV dec^{-1} without assumptions, it is reasonably postulated that nitrite reduction on the two electrodes proceeds similarly with the first electron transfer as the rate-determining step (reaction 2). The exchange current density (j_0) of nitrite reduction can be obtained by extrapolating the Tafel line to its equilibrium potential, E_{eq} = 1.45 V vs RHE.[49] The calculated j_0 values are 1.3×10^{-12} and 4.8×10^{-11} A cm^{-2} for Poly-Pd and Nano-Pd, respectively. Considering the fact that the electrochemical surface area of the Nano-Pd electrode is only around 5 times higher than that of Poly-Pd which was revealed in Figure 5, the 35 times increase of j_0 value for Nano-Pd over Poly-Pd strongly indicates that Nano-Pd is more intrinsically active than Poly-Pd, presumably because of considerable increase in the surface density of nanoscale defects-based active sites after the Poly-Pd is nanostructured into Nano-Pd.

The activity improvement caused by the surface nanostructuration is further demonstrated via the chronoamperometric measurements shown in Figure 8. Both the current−

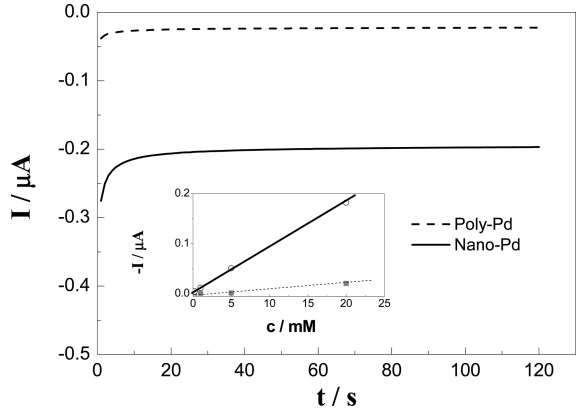

Figure 8. Current−time transients for a Nano-Pd (solid line) and a Poly-Pd (dashed line) in 0.02 mol dm^{-3} KNO_2 + 0.5 mol dm^{-3} H_2SO_4 after polarization at 0.18 V for 120 s. Inset: Dependence of steady-state currents measured at 120 s on nitrite concentration.

time transients for Nano-Pd and Poly-Pd exhibit fast current decrease at shorter times and pseudo-steady-state oxidation currents at longer times after stepping potential from 0.55 to 0.18 V. But the chronoampoermtric currents are much higher on the former. At 120 s, the steady-state currents are approximately 0.20 and 0.02 μA on Nano-Pd and Poly-Pd, respectively.

The inset to Figure 8 shows the calibration curves plotted as the nitrite concentration versus steady-state chronoamperomtric currents measured at 120 s. For the Poly-Pd electrode, a linear range is narrow with a low R^2 value of around 0.9519 and the measured sensitivity is as low as about 16 mA dm^3 cm^{-2} mol^{-1}. Nano-Pd improves the linearity of the steady-state currents and nitrite concentration relation with a high R^2 = 0.9996 value obtained over a concentration range of 0.2−20 mM, and substantially increases the sensitivity to 160 mA dm^3 cm^{-2} mol^{-1}. These suggest that nanostructuring Poly-Pd into Nano-Pd obviously improves its sensitivity and reliability to electrochemical determination of nitrite. Although this sensitivity is still lower than those of high-surface gold[47,50] and decorated carbon-nanotube electrodes,[51] the potential of Nano-Pd as a sensor electrode for nitrite detection is demonstrated for the first time through this work.

4. CONCLUSIONS

We have clearly demonstrated that the surface nanostructuration of the Poly-Pd microdisc can be conveniently achieved by applying potential cycles to mediate Zn-ECDD on the disc surface layers in an ionic liquid bath containing $ZnCl_2$ and 1-ethyl-3-methylimidazolium chloride at elevated temperature. The resulting Nano-Pd surface layers exhibit cracklike nanotextures. We propose that the development of stress induced by the incorporation and removal of Zn on the Pd surface layers during Zn-ECDD is responsible for the nanopatterning of Pd

surface layers, following a mechanism of the formation of natural crack. Highly improved responses of electrochemical oxidation of formic acid and reduction of nitrite on the Nano-Pd over Poly-Pd under similar conditions strongly suggest that the Zn-ECDD induced nanopatterning of Pd surface layers would be a convenient and green-chemistry approach to improve the activity of Pd for a wide range of potential applications from electrochemical electrocatalysis to electrochemical determination of environmental contaminants.

AUTHOR INFORMATION

Corresponding Author

*E-mail: junhua@illinois.edu.

Notes

The authors declare no competing financial interest.

REFERENCES

(1) Li, H.; Wu, N. *Nanotechnology* **2008**, *19*, 275301−5.
(2) Erlebacher, J.; Seshadri, R. *Mater. Res. Bull.* **2009**, *34*, 561−568.
(3) Zhang, J.; Li, C. *Chem. Soc. Rev.* **2012**, *41*, 7016−7031.
(4) Park, S.; Kim, H.; Chung, T. *Analyst* **2012**, *137*, 3891−3903.
(5) Lang, X.; Fu, H.; Hou, C.; Han, G.; Yang, P.; Liu, Y.; Jiang, Q. *Nat. Commun.* **2013**, *4*, 2169.
(6) Liu, H.; He, P.; Li, Z.; Li, J. *Nanotechnology* **2006**, *17*, 2167−2173.
(7) Lang, X.; Hirata, A.; Fujita, T.; Chen, M. *Nat. Nanotechnol.* **2011**, *6*, 232−236.
(8) Kim, T.; Lee, K.; Cheon, J.; Lee, J.; Joo, S.; Moon, H. *J. Am. Chem. Soc.* **2013**, *135*, 8940−8946.
(9) Erlebacher, J.; Aziz, M. J.; Karma, A.; Dimitrov, N.; Sieradzki, K. *Nature* **2001**, *410*, 450−453.
(10) Xu, C.; Wang, R.; Chen, M.; Zhang, Y.; Ding, Y. *Phys. Chem. Chem. Phys.* **2010**, *12*, 239−246.
(11) Tanaka, S.; Kaneko, T.; Asao, N.; Yamamoto, Y.; Chen, M.; Zhang, W.; Inoue, A. *Chem. Commun.* **2011**, *47*, 5985−5987.
(12) Ding, J.; Gin, D. *Chem. Mater.* **2000**, *12*, 22−24.
(13) Jiang, J.; Kucernak, A. *Electrochim. Acta* **2009**, *54*, 4545−4551.
(14) Wang, X.; Wang, W.; Qi, Z.; Zhao, C.; Ji, H.; Zhang, Z. *Electrochem. Commun.* **2009**, *11*, 1896−1899.
(15) Yi, Q.; Niu, F. *Rare Met.* **2011**, *30*, 332−336.
(16) Hakamada, M.; Nakano, H.; Furukawa, T.; Takahashi, M.; Mabuchi, M. *J. Phys. Chem. C* **2010**, *114*, 868−873.
(17) Ding, D.; Chen, Z.; Lu, C. *Sens. Actuators, B* **2006**, *120*, 182−186.
(18) Tasaltın, N.; Öztürk, S.; Kılınç, N.; Öztürk, Z. *J. Alloys Compd.* **2011**, *509*, 4701−4706.
(19) Denuault, G.; Milhano, C.; Pletcher, D. *Phys. Chem. Chem. Phys.* **2005**, *7*, 3545−3451.
(20) Bian, X.; Guo, K.; Liao, L.; Xiao, J.; Kong, J.; Ji, C.; Liu, B. *Talanta* **2012**, *99*, 256−261.
(21) Nelsona, P.; Owen, J. *J. Electrochem. Soc.* **2003**, *150*, A1313−A1317.
(22) Bartlett, P.; Gollas, B.; Guerin, S.; Marwan, J. *Phys. Chem. Chem. Phys.* **2002**, *4*, 3835−3842.
(23) Zhang, Z.; Wang, Y.; Qi, Z.; Zhang, W.; Qin, J.; Frenzel, J. *J. Phys. Chem. C* **2009**, *113*, 12629−12636.
(24) Robinson, D.; Fares, S.; Ong, M.; Arslan, I.; Langham, M.; Tran, K.; Miles Clift, W. *Int. J. Hydrogen Energy* **2009**, *34*, 5585−5591.
(25) Paillier, J.; Roue, L. *J. Electrochem. Soc.* **2005**, *152*, E1−E8.
(26) Shi, Z.; Wu, S.; Szpunar, J. *Chem. Phys. Lett.* **2006**, *422*, 147−151.
(27) Yee, C.; Jordan, R.; Ulman, A.; White, H.; King, A.; Rafailovich, M.; Sokolov, J. *Langmuir* **1999**, *15*, 3486−3491.
(28) Iben, H.; O'Brien, J. *Graph. Models* **2009**, *71*, 198−208.
(29) Skjeltorp, A.; Meakin, P. *Nature* **1988**, *335*, 424−426.
(30) Preston, S.; Griffiths, B.; Young, I. *Eur. J. Soil Sci.* **1997**, *48*, 31−37.
(31) Xia, Z.; Hutchinson, J. *J. Mech. Phys. Solids* **2000**, *48*, 1107−1131.
(32) Weh, L.; Venthur, A. *Macromol. Mater. Eng.* **2004**, *289*, 227−237.
(33) Colina, H.; Roux, S. *Eur. Phys. J. E* **2000**, *1*, 189−194.
(34) Leung, K.; Neda, Z. *Phys. Rev. Lett.* **2000**, *85*, 662−665.
(35) Ye, T.; Suo, Z.; Evans, A. *Int. J. Solids Struct.* **1992**, *29*, 2639−2648.
(36) Neda, Z.; Jarai-Szabo, F.; Kaptalan, E.; Mahnke, R. *CEAI* **2009**, *11*, 3−10.
(37) Li, J.; Dozier, A.; Li, Y.; Yang, F.; Cheng, Y. *J. Electrochem. Soc.* **2011**, *158*, A689−A694.
(38) Huang, J.; Sun, I. *Adv. Funct. Mater.* **2005**, *15*, 989−994.
(39) Jia, F.; Yu, C.; Ai, Z.; Zhang, L. *Chem. Mater.* **2007**, *19*, 3648−3653.
(40) Trasatti, S.; Petrii, O. *Pure Appl. Chem.* **1991**, *63*, 711−734.
(41) Zhu, Y.; Khan, Z.; Masel, R. *J. Power Sources* **2005**, *139*, 15−20.
(42) Rice, C.; Ha, S.; Masel, R.; Wieckowski, A. *J. Power Sources* **2003**, *115*, 229−235.
(43) Yu, X.; Pickup, P. *J. Power Sources* **2008**, *182*, 124−132.
(44) Kerkeni, S.; Lamy-Pitara, E.; Barbier, J. *Catal. Today* **2002**, *75*, 35−42.
(45) Badea, M.; Amine, A.; Palleschi, G.; Moscone, D.; Volpe, G.; Curulli, A. *J. Electroanal. Chem.* **2001**, *509*, 66−72.
(46) Cha, C.; Li, C.; Yang, H.; Liu, P. *J. Electroanal. Chem.* **1994**, *368*, 47−54.
(47) Liu, P.; Lu, J.; Yan, J. *J. Electroanal. Chem.* **1999**, *469*, 196−200.
(48) Heckner, H. *J. Electroanal. Chem.* **1973**, *44*, 9−20.
(49) Bard, A.; Parsons, R.; Jordan, J. *Standard potentials in aqueous solution*; Marcel Dekker, Inc.: New York, 1985.
(50) Liu, S.; Ju, H. *Analyst* **2003**, *128*, 1420−1424.
(51) Liu, P.; Hu, J. *Sens. Actuators, B* **2002**, *84*, 194−199.